Am J Physiol Endocrinol Metab 305: E1165–E1171, 2013.
First published September 10, 2013; doi:10.1152/ajpendo.00296.2013.

In vivo magnetic resonance of hyperpolarized [$^{13}C_1$]pyruvate: metabolic dynamics in stimulated muscle

Avigdor Leftin,[1] Hadassa Degani,[2] and Lucio Frydman[1]

[1]*Department of Chemical Physics and* [2]*Department of Biological Regulation, Weizmann Institute of Science, Rehovot, Israel*

Submitted 6 June 2013; accepted in final form 7 September 2013

Leftin A, Degani H, Frydman L. In vivo magnetic resonance of hyperpolarized [$^{13}C_1$]pyruvate: metabolic dynamics in stimulated muscle. *Am J Physiol Endocrinol Metab* 305: E1165–E1171, 2013. First published September 10, 2013; doi:10.1152/ajpendo.00296.2013.—The metabolic status of muscle changes according to the energetic demands of the organism. Two key regulators of these changes include exercise and insulin, with exercise eliciting catabolic expenditure within seconds and insulin enabling anabolic energy investment over minutes to hours. This study explores the potential of time-resolved hyperpolarized dynamic ^{13}C spectroscopy to characterize the in vivo metabolic phenotype of muscle during functional and biochemical insulin-induced stimulation of muscle. Using [$^{13}C_1$]pyruvic acid as a tracer, we find that despite the different time scales of these forms of stimulation, increases in pyruvate label transport and consumption and concomitant increases in initial rates of the tracer metabolism to lactate were observed for both stimuli. By contrast, rates of tracer metabolism to labeled alanine increased incrementally for insulin but remained unchanged following exercise-like muscle stimulation. Kinetic analysis revealed that branching of the hyperpolarized [^{13}C]pyruvate tracer between lactate and alanine provides significant tissue-specific biomarkers that distinguish between anabolic and catabolic fates in vivo according to the routing of metabolites between glycolytic and amino acid pathways.

muscle metabolism; dynamic nuclear polarization; magnetic resonance spectroscopy; insulin tolerance test; electrical muscle stimulation

MAGNETIC RESONANCE SPECTROSCOPY (MRS) in combination with stable isotope administration is one of the premiere techniques used for in vivo metabolic phenotyping in basic research, preclinical, and clinical settings. A major recent development in the field of MRS involves the use of dynamic nuclear polarization (DNP) of stable isotope-labeled markers. This hyperpolarization process bypasses the inherent low sensitivity of ^{13}C isotope tracers and has been shown to provide upwards of 10^4 signal enhancements (3), enabling fast detection of ^{13}C-labeled metabolites in vivo. These unprecedented signal gains have, for the first time, allowed measurements of metabolic fluxes in near-real time using MRS and in this fashion have provided metabolic windows into (17) in cancer (1, 20, 22), cardiovascular (33), and hepatic research (27).

Identifying unique in vivo biomarkers in muscle using hyperpolarized ^{13}C stable isotope MRS is an important and unrealized goal that could enable preclinical and clinical investigation of metabolic muscle homeostasis and disease. In this study, we explored the potential of hyperpolarized [$^{13}C_1$]pyruvate (23) as tracer to access initial rates of multiple metabolic pathways under biochemical and physical stimulation of muscle. The hyperpolarized [$^{13}C_1$]pyruvate acts as a classical isotope tracer, albeit with a finite lifetime of the observable signal, that reports on the state of the prepared metabolic system by probing intracellular transport and initial forward rates of $^{13}C_1$ label conversion of the substrate to labeled products, as determined by the enzyme-mediated flux between metabolite pools. Toward this end, we chose two paradigmatic stimulators of anabolic and catabolic muscle metabolism, insulin and exercise, respectively. These metabolic cues elicit the anabolic or catabolic responses by changing the flux of metabolites and triggering protein signaling events that can affect metabolic rates. Since MRS using stable isotope polarization is an emerging physiological technique, our primary aim in performing these manipulations was to *1*) test whether the regulatory influence of these stimuli on metabolite transport could be used to increase intracellular hyperpolarized tracer availability and *2*) monitor changes of intracellular fluxes and kinetic responses to define in vivo signatures representative of canonical anabolic and catabolic fates.

Hyperpolarized ^{13}C-MRS of pyruvate could provide a window into the metabolic fates in skeletal muscle, thanks to its unique positioning at the branching point of multiple metabolic pathways, as shown in Fig. 1. Pyruvate is produced following dephosphorylation of a key regulatory enzyme of glycolysis: pyruvate kinase. As a metabolic tracer, pyruvate enables the monitoring of downstream metabolic pathways via its products lactate, alanine, and bicarbonate. [$^{13}C_1$]lactate produced via NADH-dependent hydrolysis of [$^{13}C_1$]pyruvate by lactate dehydrogenase (LDH) reports on an end point in the glycolytic pathway (9, 16). [$^{13}C_1$]alanine synthesized by glutamate-dependent transamination of [$^{13}C_1$]pyruvate as catalyzed by the muscle-specific isoform of alanine transaminase [alanine transaminase type 2 (ALT2)] (25) is a tracer of endogenous amino acid (AA) production that fuels anabolic biomolecular synthesis, anaplerosis of the tricarboxylic acid (TCA) cycle via the α-ketoglutarate (α-KG) product, and gluconeogenesis (14). Acetyl-CoA formed following decarboxylation of [$^{13}C_1$]pyruvate by the pyruvate dehydrogenase complex prior to TCA metabolism in the mitochondria can also give rise to a [$^{13}C_1$]bicarbonate spectral signature (34).

Over the course of this study, DNP-enhanced ^{13}C-MRS revealed significant muscular metabolic responses during insulin tolerance tests and upon varying durations of functional electric stimulation of both sciatic nerves. Increases in muscle utilization of [$^{13}C_1$]pyruvate were observed via changes in metabolite-to-total carbon ratios (MtoC) for functional and insulin stimulation; intracellular transport of this glycolytic product and AA precursor increased even within just a few seconds of the electric stimulus. Additional evidence of enhanced glycolytic metabolism stems from the kinetic rates of [$^{13}C_1$]lactate formed from [$^{13}C_1$]pyruvate, which increased threefold for maximal insulin stimulation and sixfold after 30

Address for reprint requests and other correspondence: L. Frydman, Dept. of Chemical Physics, Weizmann Institute of Science, 76100 Rehovot, Israel (e-mail: lucio.frydman@weizmann.ac.il).

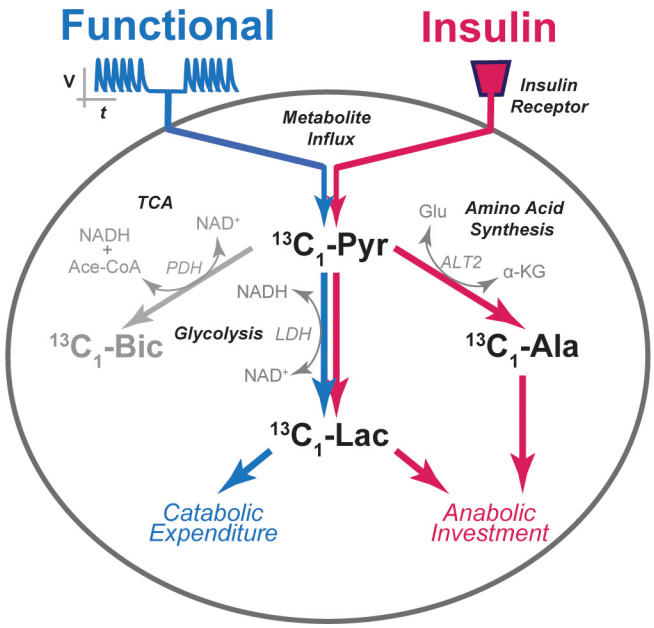

Fig. 1. Potential paths whereby hyperpolarized ^{13}C-MRS can probe in vivo metabolic response to skeletal muscle stimulation. Electrical nerve stimulation mimicking exercise or insulin hormone binding to cell receptors elicits different metabolic responses in muscle. Our experiments reveal that hyperpolarized [^{13}C$_1$]pyruvate (^{13}C$_1$-Pyr) and its main observable metabolic products [^{13}C$_1$]lactate (^{13}C$_1$-Lac) and [^{13}C$_1$]alanine (^{13}C$_1$-Ala) trace metabolic transport and enzymatic reactions within glycolytic and amino acid synthesis pathways under these canonical stimuli (colored arrows). Glu, glutamate; ALT2, alanine transaminase type 2; α-KG, α-ketoglutarate; ^{13}C$_1$-Bic, [^{13}C$_1$]bicarbonate; Ace-CoA, acetyl-CoA; LDH, lactate dehydrogenase; PDH, pyruvate dehydrogenase.

s of nerve stimulation. By contrast, [^{13}C$_1$]alanine rates changed progressively, reaching increases of threefold during the insulin tolerance test, but increased only slightly and thereafter remained constant for different durations of functional stimulation. We show that the difference in metabolic response can be related to the kinetic branching behavior of the hyperpolarized pyruvate tracer between glycolytic and AA pathways. This dynamic indicator gauges the ability of muscle to direct metabolic flux between anabolic and catabolic fates, depending on the instantaneous metabolic requirement.

MATERIALS AND METHODS

Magnetic resonance experiments. In vivo magnetic resonance imaging and spectroscopy were conducted on a 4.7-T (30-cm bore) spectrometer system (Biospec; Bruker). A double-resonance 20-mm ^{1}H/^{13}C surface coil probe was used. ^{1}H gradient echo reference images were obtained to confirm positioning of the animal for detection of hindlimb skeletal muscle (including vasti, soleus, and gastrocnemius muscles) once the animal was secured on the surface coil bed. Dynamic ^{13}C spectra were acquired for 256 sequential acquisitions (2,048 time domain points per acquisition, over a 10-kHz spectral bandwidth), with an interscan repetition of 1 s and a broadband radio frequency pulse flip angle of 15°. Each time trace was zero-filled to 4,096 points, Fourier transformed, processed with a Gaussian apodization using the manufacturer's software (Paravision 4.0; Bruker), and further analyzed using Matlab (Mathworks) routines.

DNP. Hyperpolarization of [^{13}C$_1$]pyruvic acid (Sigma Isotec) co-dissolved with OXO-63 radical (GE HealthCare) at a ratio of 58:1 wt/wt and was conducted at 95 GHz with 50 mW of microwave power in a Hypersense polarizer (GE HealthCare), operating at 1.5 K and yielding solid-state enhancements of ~8,000-fold with average buildup times of 725 s. Hyperpolarized samples transferred directly to the imaging magnet had solution state spin polarizations of ~22%.

Animals. Animal protocols and maintenance were in accordance with the guidelines of the Committee on Animals of the Weizmann Institute of Science and were approved by this committee. Female 8-wk-old ICR mice were maintained in nonreversed light conditions and provided with standard chow and water ad libitum prior to the experiments.

Insulin tolerance tests. Animals were anesthetized during feeding hours (6 PM to 12 AM) with 50 mg/kg pentobarbital sodium, and the tail vein was cannulated. Animals were secured in the magnet and maintained with 1–2% isoflurane in O_2 at 1 l/min. Insulin tolerance tests were initiated with a 100-μl intraperitoneal injection of 0.3 U/kg human insulin (Sigma) injection. Hyperpolarized tracer experiments were conducted on the statistical cohort by making individual measurements on separate animals for control 0 min, 15 min, 30 min, and 60 min post-insulin injection (n = 4/time point) using 300-μl doses of 60 mM [^{13}C$_1$]pyruvic acid dissolved in pH ≈ 7.6 buffer containing 60 mM NaOH, 40 mM Trizma-PreSet, pH = 7.6, 0.1 g/l EDTA, and isotonic NaCl. Plasma-based insulin tolerance tests were conducted by tail sampling of blood glucose of the anesthetized animal with a blood glucose meter (AccuCheck) following insulin injection at the same time intervals used in the hyperpolarized experiments.

Electrical stimulation of sciatic nerve. Muscular function was implemented via electrical nerve stimulation (26). To this end, animals were anesthetized during feeding hours (6 PM to 12 AM) with 70 mg/kg pentobarbital sodium. The sciatic nerves of the hindlimbs were exposed by small surgical incisions. Hooked cathode leads were fastened around the nerve, and the incision was closed by suture tape. Anode leads were then inserted into the hindfoot pads and secured. The tail vein was cannulated, and the animal was fixed in position in the magnet and maintained with 1–2% isoflurane in O_2 at 1 l/min. The supramaximal electrical stimulation paradigm consisted of 10-millisecond trains of 200-microsecond square pulses played at a repetition frequency of 10 Hz with a positive amplitude of 15 V. Stimulation was applied for durations of 15, 30, and 90 s, and hyperpolarized experiments were conducted on the statistical cohort by making individual measurements on separate animals before (t = 0) and immediately following the stimulation for each time point (n = 4/time point) using 300-μl doses of 60 mM [^{13}C$_1$]pyruvic acid dissolved in pH ≈ 7.6 buffer containing 60 mM NaOH, 40 mM Trizma-PreSet, pH = 7.6, 0.1 g/l EDTA, and isotonic NaCl.

Magnetic resonance spectral analysis. Metabolite peaks observed in each spectrum were integrated by trapezoidal numeric approximation of the exact integral using Matlab (Mathworks) over their respective spectral frequency band. The total area per spectrum was found by summing the total metabolite peak areas. The normalized MtoC ratios for each metabolite were determined per spectral acquisition and also for summations of all spectra acquired per experiment by dividing each metabolite peak integral area by the total carbon integral area.

Kinetic rates I: Bloch equations analysis. The time rate of change of the integral areas of each metabolite follows the change of longitudinal magnetization of [^{13}C$_1$]pyruvate $M_z^{Pyr}(t)$, [^{13}C$_1$]lactate $M_z^{Lac}(t)$, and [^{13}C$_1$]alanine M_z^{Ala}, as described by the Bloch-McConnell formalism. These coupled differential equations depend on the spin lattice relaxation rate for each metabolite R_1, the pulse flip angle θ_p, the interscan repetition time TR, and the metabolic rate k for the forward conversion of Pyr to Lac k_{Lac} and from Pyr to Ala k_{Ala}. Their differential form is

$$\dot{M}_z^{Pyr}(t) = -M_z^{Pyr}(t)\left(R_1^{Pyr} + k_{Lac} + k_{Ala} + \left(1 - \cos(\theta_p)\right)/TR\right) \quad (1)$$

$$\dot{M}_z^{Lac}(t) = M_z^{Pyr}(t)k_{Lac} - M_z^{Lac}(t)\left(R_1^{Lac} + \left(1 - \cos(\theta_p)\right)/TR\right) \quad (2)$$

$$\dot{M}_z^{Ala}(t) = M_z^{Pyr}(t)k_{Ala} - M_z^{Ala}(t)\left(R_1^{Ala} + \left(1 - \cos(\theta_p)\right)/TR\right) \quad (3)$$

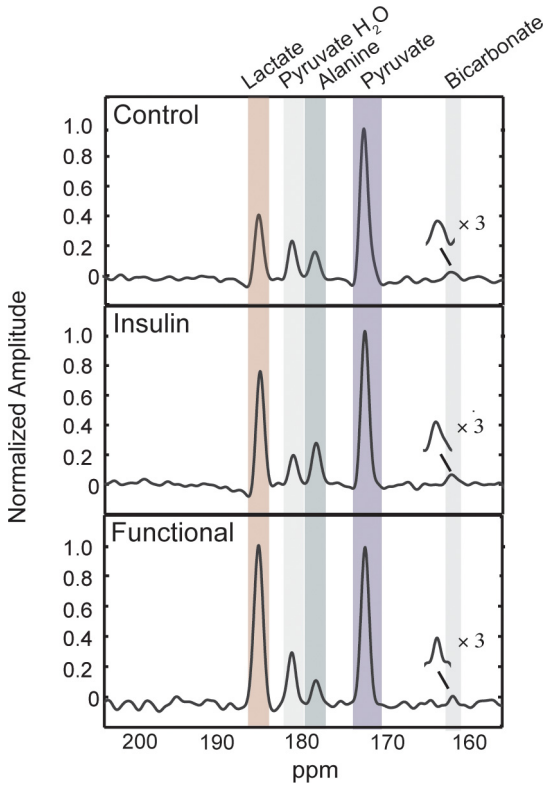

Fig. 2. Changes measured by hyperpolarized ^{13}C-MRS in response to insulin and a functional model of exercise. ^{13}C-MRS spectra obtained following the injection of [^{13}C$_1$]pyruvate for control (*top*), insulin dosed at 30 min (*middle*), and exercised hindlimb skeletal muscle following 30 s of electrical sciatic nerve stimulation (*bottom*). The shown spectra are the summations of all 256 acquisitions collected 1 s apart during the dynamic ^{13}C-MRS experiment. The peak areas (shaded regions) for observed metabolites ^{13}C$_1$-Pyr, ^{13}C$_1$-Ala, ^{13}C$_1$-Lac, and ^{13}C$_1$-Bic and the nonmetabolically active ^{13}C$_1$-Pyr hydrate were determined and used to obtain the kind of data shown in Figs. 3–7.

Notice that solely unidirectional reaction kinetics are considered, given the large excess of the [^{13}C$_1$]pyruvate precursor. These equations were solved, and kinetic data (normalized by the initial Pyr signal) was fit either by using numerical minimizations against the coupled set of differential equations or by fitting their analytic solutions in Matlab.

Kinetic rates II: initial rate analysis. The normalized MtoC ratios were also used to calculate the rates during the initial 30 s following injection of [^{13}C$_1$]pyruvate. The kinetic curves calculated in this interval follow monoexponential behavior, which is characteristic of a noncompetitive parallel rate law (4). In the approximation that the nuclear spin relaxation rates (R_1) of all hyperpolarized magnetizations are equal in this initial time frame, and that so are the pulse flip angle θ_p and the *TR*-dependent contributions, the only factor influencing MtoC ratios becomes the metabolic rates k_{Lac} and k_{Ala}. Indeed, in such a case the coupled set of equations (*Eqs. 1–3*) can be simplified to

$$\mathrm{MtoC}^{\mathrm{Pyr}}(t)/\mathrm{d}t = -\mathrm{MtoC}^{\mathrm{Pyr}}(t)\left(k_{\mathrm{Lac}} + k_{\mathrm{Ala}}\right) \quad (4)$$

$$\mathrm{MtoC}^{\mathrm{Lac}}(t)/\mathrm{d}t = \mathrm{MtoC}^{\mathrm{Pyr}}(t)k_{\mathrm{Lac}} \quad (5)$$

$$\mathrm{MtoC}^{\mathrm{Ala}}(t)/\mathrm{d}t = \mathrm{MtoC}^{\mathrm{Pyr}}(t)k_{\mathrm{Ala}} \quad (6)$$

Initial kinetic rates were also obtained in this fashion either by numerical minimizations or by fitting analytical solutions of *Eqs. 4–6* to the experimental data using Matlab.

RESULTS

In vivo hyperpolarized ^{13}C-MRS characterizes metabolic changes in stimulated skeletal muscle. Tracer experiments of hyperpolarized [^{13}C$_1$]pyruvate enable the measurement of the metabolic processes depicted in Fig. 1 for muscle subject to chemical (insulin) or functional (electrical) stimulation. Representative spectra evidencing this are shown in Fig. 2. These traces are shown for control animals (Fig. 2, *top*), following 30 min of insulin action (Fig. 2, *middle*), or following 30 s of supramaximal sciatic nerve stimulation (Fig. 2, *bottom*). Signals for hyperpolarized [^{13}C$_1$]pyruvate, [^{13}C$_1$]pyruvate hydrate, and metabolic products [^{13}C$_1$]lactate, [^{13}C$_1$]alanine, and [^{13}C$_1$]bicarbonate were observed in all of these muscle measurements. In the following, we treat only the changes in [^{13}C$_1$]pyruvate, [^{13}C$_1$]lactate, and [^{13}C$_1$]alanine, as the low signal-to-noise ratio observed for the [^{13}C$_1$]bicarbonate resonance precluded obtaining statistically significant measurements within the cohort.

Integral areas were calculated for the shaded frequency bands shown in Fig. 2 to quantify the evident changes visible in the spectra, and MtoC ratios were calculated using these integrals obtained over the course of the tracer experiment. First, we compared MtoCs with changes of blood glucose during standard insulin tolerance tests (5) conducted under the same experimental conditions. Insulin tolerance tests have determined that the hormone has a plasma half-life of ~15 min (11), suggesting that response extremes should be observed at ~30 min postinjection. Indeed, Fig. 3 shows that there is a relative change of blood glucose as well as [^{13}C$_1$]pyruvate that traces the increased disposal of metabolic fuel to the muscle tissue. Unique to the DNP tolerance test, however, are the intracellular metabolic changes evidenced by increases in [^{13}C$_1$]alanine and [^{13}C$_1$]lactate.

The MtoC peak ratios for [^{13}C$_1$]pyruvate, [^{13}C$_1$]lactate, and [^{13}C$_1$]alanine for both insulin and high-intensity muscle function, as achieved by in vivo sciatic nerve stimulation of both hindlimbs, are shown in Fig. 4. For insulin, pyruvate MtoC decreases significantly at 15 min and even further after 30 min, whereas at 60 min the pyruvate MtoC begins to recover. In the functional hyperpolarized [^{13}C$_1$]pyruvate experiments, pyruvate's MtoCs reduce significantly following a short 15-s bout of supramaximal exercise and continue to fall toward the exhaustion limit at 30 s; these changes parallel those observed for insulin, albeit on a signifi-

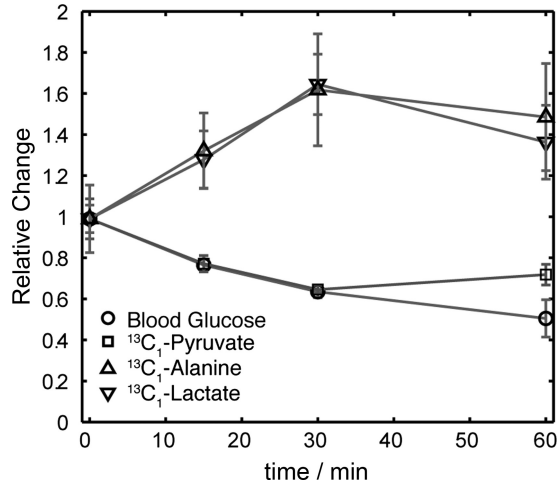

Fig. 3. Comparison of hyperpolarized and standard insulin tolerance tests. The relative change for blood glucose (○), metabolite-to-total carbon ratios (MtoC) of hyperpolarized ^{13}C$_1$-Pyr (□), hyperpolarized ^{13}C$_1$-Ala (△), and hyperpolarized ^{13}C$_1$-Lac (▽) at 15, 30, and 60 min following administration of 0.3 U/kg insulin at 0 min.

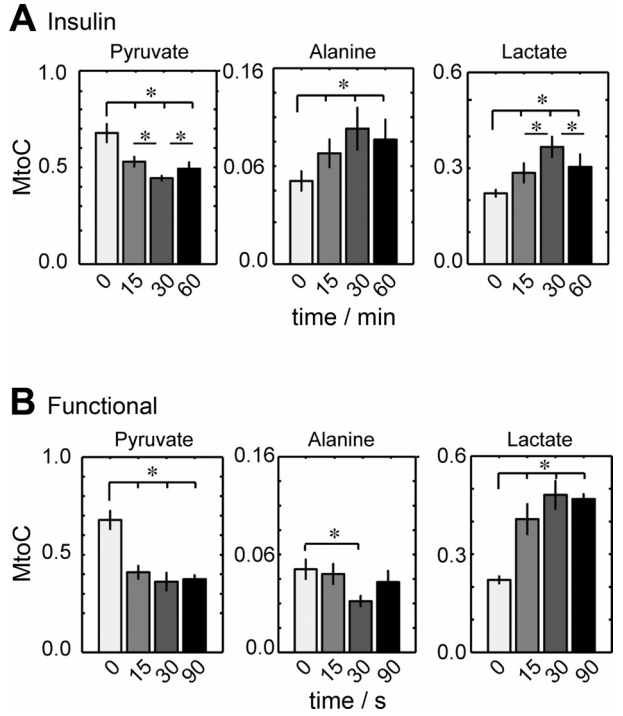

Fig. 4. MtoC for $^{13}C_1$-Pyr, $^{13}C_1$-Ala, and $^{13}C_1$-Lac. Insulin dose response at 0, 15, 30, and 60 min (*A*), and 0, 15, 30, and 90 s of functional stimulation (*B*). Statistical significance (*$P < 0.05$) for differences in time points with respect to control was determined using a 2-tailed *t*-test ($n = 4$/measurement).

cantly different time scale. These DNP MRS results suggest that the pyruvate tracer consumption increases with stimulation of intracellular flux. This is substantiated by previous in vivo ^{31}P measurements using the same exercise paradigm (26) reporting that the first 30 s of this stimulation lead to depletion of the phosphocreatine pool and steady-state ATP reserve, thereby necessitating increases in the glucose pool to provide metabolic fuel to the tissue. Interestingly, alanine and lactate MtoCs in this functional stimulation do not obey similar trends as for insulin; whereas for lactate a stepwise increase is observed for 15 and 30 s, reaching a plateau at 90 s, alanine exhibits little variation for the all durations. These tissue-specific in vivo muscle measurements show that metabolite pools of both lactate and alanine can populate in proportion to the available intracellular [$^{13}C_1$]pyruvate tracer yet exhibit marked variation depending on the type of stimulation.

In vivo kinetic analysis shows similar poststimulus rates for pyruvate metabolism and lactate synthesis but differences in alanine synthesis. A main advantage of hyperpolarized ^{13}C-MRS experiments is that kinetics of metabolic pathways become amenable to measurements in a near-real-time fashion. This aspect is crucial for recording tissue-specific metabolic responses, for instance, in this case muscular responses to insulin and function, because such stimuli can cause changes that are dynamic over short time scales. This precludes the use of standard in vivo techniques, including MRS methods (7) that have thus far provided insight into [^{13}C]glycogen accumulation under varied insulinemic conditions over the course of hours (28, 35), and metabolite usage following long bouts of exercise (8). Figure 5 shows representative examples of the kind of tracer dynamics that hyperpolarized ^{13}C-MRS can deliver for [$^{13}C_1$]pyruvate and metabolic products [$^{13}C_1$]lactate and [$^{13}C_1$]alanine for control animals (Fig. 5, *top*), after 30 min of insulin dosing (Fig. 5, *middle*), and following 30 s of sciatic nerve stimulation (Fig. 5, *bottom*). The peak signal of the injected [$^{13}C_1$]pyruvate tracer is first reached, and this is followed by the buildup and subsequent decay of both [$^{13}C_1$]lactate and [$^{13}C_1$]alanine signals. All of these time series can be quantitatively fit by *Eqs. 1–3* to extract the intracellular rates of LDH and ALT2 enzymatic reactions. Figure 6 illustrates the changes undergone by these rates as a function of the insulin and functional stimulation times. These rate changes follow the same trends as observed for the MtoC values. The changes of metabolic rates suggest that intracellular flux of the pyruvate substrate has increased for both stimuli. For insulin, this contributes to significant threefold increases in alanine, and lactate metabolic rates are observed. Similarly, for functional stimulation, lactate metabolism increases progressively and reaches sixfold over control. In contrast with insulin, however, rates of alanine metabolism are increased but remain nearly constant for the exercise durations considered.

Branching behavior of the initial rates observed by ^{13}C-MRS reflects the metabolites' anabolic and catabolic fates. Whereas our experiments show that during insulin stimulation glycolytic and AA production are similarly changed to accommodate the increased availability of metabolic fuel, muscular exercise appears to favor glycolysis at the expense of alanine synthesis. Such differences are reflected in the dynamic changes observed

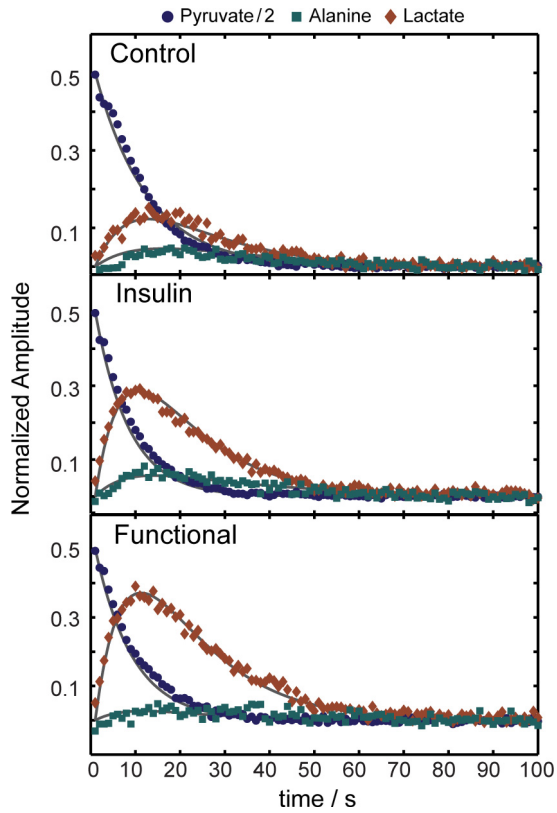

Fig. 5. In vivo postinjection kinetics revealed by hyperpolarized $^{13}C_1$-Pyr for the insulin and functional stimuli. The traces reflect representative changes in hyperpolarized signal observed following injection of $^{13}C_1$-Pyr for control (*top*), insulin dosed at 30 min (*middle*), and and 30 s of functional stimulation (*bottom*). Overlaying the $^{13}C_1$-Pyr (blue circles), $^{13}C_1$-Ala (green squares), and $^{13}C_1$-Lac signals (red diamonds) are best fits to the Bloch-McConnell *Eqs. 1–3* (solid lines).

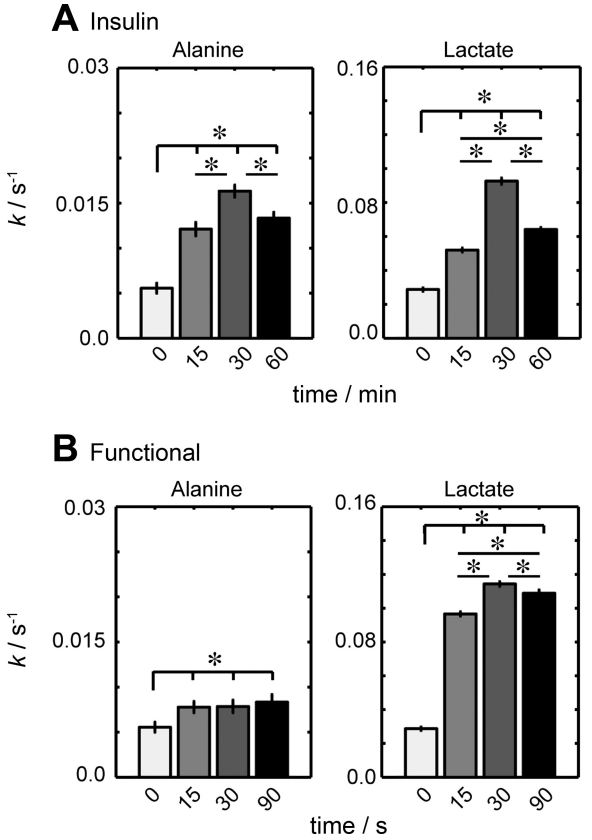

Fig. 6. In vivo kinetic rates deriving from numerical fits of the Bloch-McConnell equations for $^{13}C_1$-Ala and $^{13}C_1$-Lac in stimulated muscle. *A*: insulin dose response at 0, 15, 30, and 60 min following administration of 0.3 U/kg insulin. *B*: functional response following 0, 15, 30, and 90 s of functional stimulation. Statistical significance (*$P < 0.05$) for differences in time points with respect to control was determined using a 2-tailed *t*-test ($n = 4$/measurement).

for kinetic rates of pyruvate-to-lactate and pyruvate-to-alanine conversion. In this sense, both Figs. 4 and 6 show that the routing of pyruvate between glycolytic and AA pathways is changed during these anabolic and catabolic model responses. However, although suggestive of a metabolic switch that is of biological origin that genuinely reflects system regulation of metabolic tracer fate, as has been observed in in vitro assays (2, 6), another possibility arises; i.e., the depopulation of the alanine pathway in the functional test could also be an artifact of the tracer experiment that results from a reduced availability of pyruvate due to a greatly increased lactate production.

To discriminate between these two alternatives, kinetic traces recorded during the first 30 s following tracer injection were analyzed according to parallel rate laws introduced in *Eqs. 4–6*, and initial rates were determined. These normalized models, which factor out common relaxation decays, lead to the best fits of the experimental data shown in Fig. 7*A* for [$^{13}C_1$]pyruvate, [$^{13}C_1$]lactate, and [$^{13}C_1$]alanine tracer dynamics. These initial rate plots are shown for control (Fig. 7*A*, *top*), at 30 min postinsulin (Fig. 7*A*, *middle*), and post-nervous stimulation for 30 s (Fig. 7*A*, *bottom*). The discriminating feature between a parallel, noncompetitive rate law and competitive behavior is given by the branching ratio between lactate- and alanine-generating reaction rates. For a noncompetitive case, the ratio of the lactate-to-alanine MtoC exhibits a positive slope, as observed in the experimental data, whereas for a classical parallel competitive system, the branching ratio is strictly constant (slope = 0) over the course of the kinetic experiment. Experimentally, we observed that the pyruvate is consumed at a rate determined by its metabolism to lactate and alanine, whereas the monoexponential buildup of lactate and alanine is determined by the initial forward rate of each metabolic reaction independently, leading to a positive slope. Thus, on the basis of the results observed in Figs. 7*A*, we conclude that the initial rates measured represent legitimate markers, distinguishing between anabolic and catabolic fates in vivo.

Figure 7, *B* and *C*, complements this information by depicting the evolution of these branching dynamics as a function of the time elapsed after insulin dosing or functional stimulation duration. As shown in Fig. 7*B*, the ratios of lactate to pyruvate and of alanine to pyruvate, as well as the branching of pyruvate between lactate and alanine, remain nearly constant over the course of the insulin tolerance test. By contrast, as shown in Fig. 7*C*, the exercise paradigm differentially affects the ratios of these rates, with lactate-to-pyruvate and lactate-to-alanine ratios increasing and alanine-to-pyruvate ratio decreasing. These specific changes suggest that exercising muscle favors the routing of metabolic fuel toward catabolic generation of energy as the glycolytic end point lactate rather than alanine.

DISCUSSION

This study demonstrates for the first time that quantitative kinetics can be measured in vivo for skeletal muscle during rest, under hormonal stimulation, and following nerve stimulation mimicking exercise for multiple metabolic reactions using the enhanced sensitivity afforded by hyperpolarized [$^{13}C_1$]pyruvate MRS. In addition to the signal gains achieved, a key advantage of hyperpolarized ^{13}C spectroscopy is that it enables kinetic rates to be measured in real time; for our experiments, 30 s of tracer measurement was sufficient to determine the unidirectional rates for the enzyme-mediated metabolism of [$^{13}C_1$]pyruvate to [$^{13}C_1$]lactate and [$^{13}C_1$]alanine using a classical noncompetitive parallel rate law formalism. This represents a significant advance for MRS isotope studies utilizing ^{13}C tracers, since acute response to metabolic challenge and repeated kinetic rate determinations are now achievable during protocols that have been previously been restricted to long measuring times due to the low sensitivity of the conventional ^{13}C experiment.

Muscle stimulation enables tracer transport and affects intracellular metabolic flux. Muscle metabolism requires an influx of precursor metabolites to fuel the tissue's energy requirements. Muscle tissue is the main consumer of glucose, and both exercise and insulin facilitate the entry of this metabolic fuel via translocation of vesicular glucose transporters, primarily GLUT4, to the cell membrane (13, 24). Similarly, monocarboxylate (10, 29) and amino acid (32) transporters are activated by both stimuli, facilitating the influx of metabolic fuels and the efflux of metabolic products from muscle cells. Especially important for functional stimulation is blood flow (19) that can increase availability of metabolites to muscle tissue. Consideration of these physiological responses in the context of hyperpolarized ^{13}C-MRS suggested that not only could we utilize the method to provide near-real-time metabolic rates, but also, we could explore the possibility of using hormonal and functional stimulation to increase the rate of

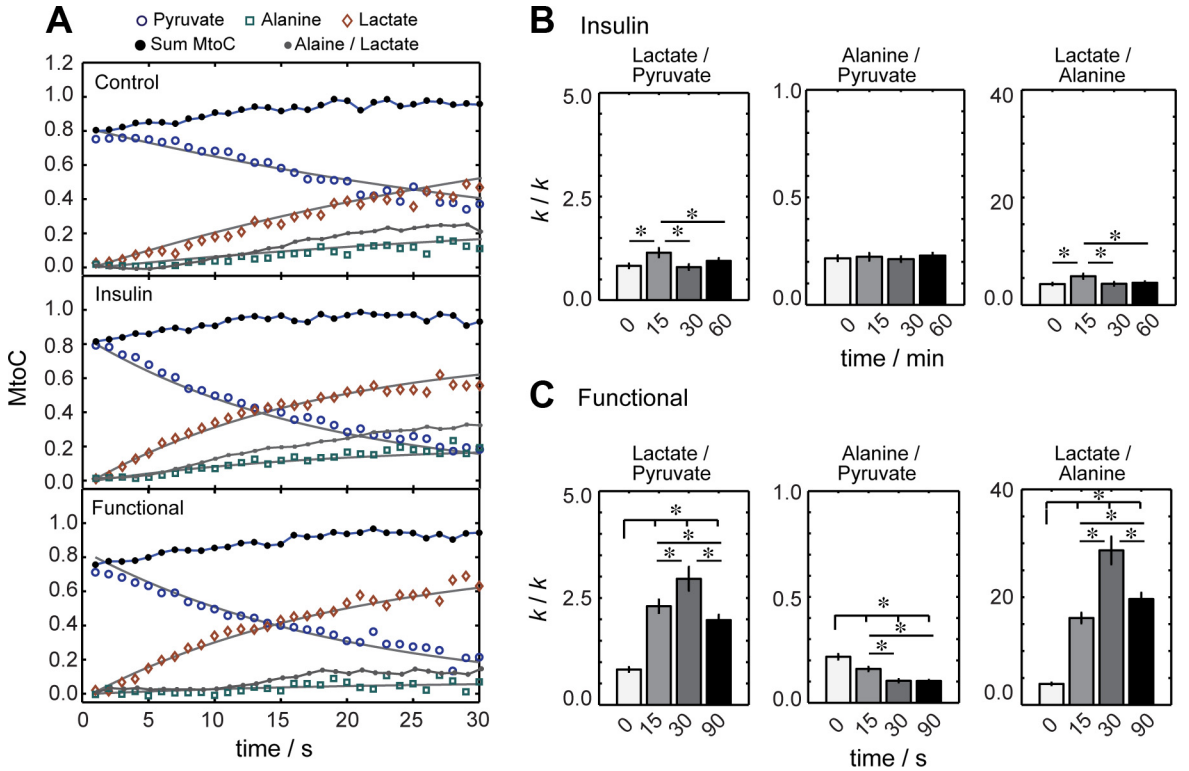

Fig. 7. Initial rates of parallel tracer kinetics show branching behavior of pyruvate between lactate and alanine metabolic pathways. *A*: MtoC traces for $^{13}C_1$-pyruvate (blue open circles), $^{13}C_1$-Ala (green open squares), and $^{13}C_1$-Lac during the first 30 s following peak $^{13}C_1$-Pyr signal appearance (red open diamonds) follow a parallel kinetics rate law, as shown by best fit (solid line). Initial rates are shown for control (*top*), 30 min post-insulin dosing (*middle*), and immediately after 30 s of functional stimulation (*bottom*). Sum metabolite-to-total carbon ratios (●) remain approximately constant over the initial rate duration. The branching ratios of alanine to lactate (gray circles) exhibit positive slopes characteristic of a noncompetitive parallel reaction system. *B* and *C*: branching ratios of initial kinetic rates lactate/pyruvate (*left*), alanine/pyruvate (*middle*), and lactate/alanine (*right*) for insulin dose response at 0, 15, 30, and 60 min following administration of 0.3 U/kg insulin (*B*) and following 0, 15, 30, and 90 s of sciatic nerve stimulation (*C*).

tracer transport since this is a potentially rate-limiting step for both signal detection and observation of metabolic reactions. Indeed, changes in the areas of the hyperpolarized [$^{13}C_1$]pyruvate signals show that conditionally dependent fluxes can be initiated under stimulation that must initially be regulated by transporters on the seconds-to-minutes timescale.

Regulation of the influx and efflux of metabolites within glycolytic, the tricarboxylic acid cycle, and amino acid synthesis routes (16, 21, 32) is ensured by translation, phosphorylation events, and enzymatic cofactors. During the insulin tolerance test, phosphorylation events in the PI3K/mTOR/Akt signaling pathway (12, 18) stimulate anabolic muscle metabolism to provide mainly for storing glucose as glycogen and ATP production via aerobic glycolysis and the TCA cycle as well as synthesis of amino acids for sustaining biomolecular assembly and liver gluconeogenesis (12). Anabolic stimulation by insulin causes parallel increases of LDH and ALT flux, as indicated by the trend in the metabolic rates for the hyperpolarized $^{13}C_1$ tracer. For exercise that can be carried out through functional electrical stimulation of sciatic nerve, the metabolic system responds by coupling AMPK activation to changes in the AMP/ATP equilibrium (30, 31, 36). This upregulates glycolytic catabolism (36) and downregulates fatty acid inputs into the TCA cycle (8). The increase in glucose catabolism during functional stimulation is indicated by increases in the initial rates of [$^{13}C_1$]pyruvate metabolism to [$^{13}C_1$]lactate via the LDH reaction. Dynamic muscular exercise causes decreases in intramuscular glutamate that subsequently keep α-KG, an anaplerotic metabolite produced alongside alanine in the ALT reaction, nearly constant (15). This mirrors the insignificant changes in initial metabolic rates of [^{13}C]alanine conversion from [^{13}C]pyruvate obtained in the same enzymatic reaction. Overall, the signatures of these regulatory mechanisms arising from the two canonical stimuli applied in our experiments are the kinetic branching ratios between [$^{13}C_1$]pyruvate flux through [$^{13}C_1$]lactate and [$^{13}C_1$]alanine reactions, a constant kinetic branching ratio being observed over the course of the insulin tolerance test, and a glycolytically biased branching ratio for varying durations of functional challenge.

CONCLUSIONS

This study demonstrates that metabolic response to functional exercise and hormonal stimulation of skeletal muscle is detectable nearly in real time using in vivo hyperpolarized ^{13}C spectroscopy. These functional and insulin stimulations of muscle cause marked and highly significant changes to multiple metabolic reactions, providing anabolic and catabolic biomarkers within a 30-s experiment. The instantaneous changes caused by metabolic challenge that are observable in the hyperpolarized ^{13}C experiments reflect regulation events governing metabolic transport and initial-rate kinetics. The kinetic responses and dynamic branching behavior probed by hyperpolarized [$^{13}C_1$]pyruvate can be used to gauge the metabolic

sensitivity of the organism and lend insight into systems changes caused by the onset and progression of metabolic syndromes. To this end, we are currently pursuing such metabolic data for genetically modified animals, exploring additional ^{13}C substrates to extend our reach to TCA and fatty acid metabolic processes, and developing spectroscopic and imaging techniques that efficiently use hyperpolarized signals.

ACKNOWLEDGMENTS

We thank Atan Gross, Nava Nevo, and Koby Zibzener for discussions and assistance with these experiments.

GRANTS

Financial support from the Deutsch-Israelische Projektkooperation (German-Israeli Project Cooperation) Project 710907 (Ministry of Education and Research, Germany), the European Union (through European Research Council Advanced Grant No. 246754), and a Helen and Kimmel Award for Innovative Investigation and the generosity of the Perlman Family Foundation are gratefully acknowledged. A. Leftin is also grateful to the Fulbright Program and to the US National Science Foundation International Postdoctoral Fellowship Program for their respective awards.

DISCLOSURES

No conflicts of interest, financial or otherwise, are declared by the authors.

AUTHOR CONTRIBUTIONS

A.L., H.D., and L.F. contributed to the conception and design of the research; A.L. performed the experiments; A.L. analyzed the data; A.L., H.D., and L.F. interpreted the results of the experiments; A.L. prepared the figures; A.L. drafted the manuscript; A.L., H.D., and L.F. edited and revised the manuscript; A.L., H.D., and L.F. approved the final version of the manuscript.

REFERENCES

1. **Albers MJ, Bok R, Chen AP, Cunningham CH, Zierhut ML, Zhang VY, Kohler SJ, Tropp J, Hurd RE, Yen Y, Nelson SJ, Vigneron DB, Kurhanewicz J.** Hyperpolarized ^{13}C lactate, pyruvate, and alanine: noninvasive biomarkers for prostate cancer detection and grading. *Cancer Res* 68: 8607–8615, 2008.
2. **Aragón JJ, Lowenstein JM.** The purine-nucleotide cycle. Comparison of the levels of citric acid cycle intermeidates with the operation of the purine nucleotide cycle in rat skeletal muscle during exercise and recovery from exercise. *Eur J Biochem* 110: 371–377, 1980.
3. **Ardenkjaer-Larsen JH, Fridlund B, Gram A, Hansson G, Hansson L, Lerche MH, Servin R, Thaning M, Golman K.** Increase in signal-to-noise ratio of $>$ 10,000 times in liquid-state NMR. *Proc Natl Acad Sci USA* 100: 10158–10163, 2003.
4. **Atkins PW, de Paula J.** *Physical Chemistry* (7th ed.). New York: Freeman, 2002.
5. **Ayala JE, Samuel VT, Morton GJ, Obici S, Croniger CM, Shulman GI, Wasserman DH, McGuinness OP.** Standard operating procedures for describing and performing metabolic tests of glucose homeostasis in mice. *Dis Model Mech* 3: 1–10, 2012.
6. **Bangsbo J, Gibala MJ, Howarth KR, Krustrup P.** Tricarboxylic acid cycle intermediates accumulate at the onset of intense exercise in man but are not essential for the increase in muscle oxygen uptake. *Pflügers Arch* 452: 737–743, 2006.
7. **Befroy DE, Petersen KF, Rothman DL, Shulman GI.** Assessment of in vivo mitochondrial metabolism by magnetic resonance spectroscopy. *Meth Enzymol* 457: 373–393, 2009.
8. **Bertocci LA, Jones JG, Malloy CR, Victor RG, Thomas GD.** Oxidation of lactate and acetate in rat skeletal muscle: analysis by ^{13}C-nuclear magnetic resonance spectroscopy. *J Appl Physiol* 83: 32–39, 1997.
9. **Brooks GA.** Cell-cell and intracellular lactate shuttles. *J Physiol* 587: 5591–5600, 2009.
10. **Coles L, Litt J, Hatta H, Bonen A.** Exercise rapidly increases expression of the monocarboxylate transporters MCT1 and MCT4 in rat muscle. *J Physiol* 561: 253–261, 2004.
11. **Coore HG, Westman S.** Disappearance of serum insulin in obese-hyperglycemic mice. *Acta Physiol Scand* 78: 274–279, 1970.
12. **Dimitriadis G, Mitrou P, Lambadiari V, Maratou E, Raptis SA.** Insulin effects in muscle and adipose tissue. *Diabetes Res Clin Pract* 935: S52–S59, 2011.
13. **Egan B, Zierath JR.** Exercise metabolism and the molecular regulation of skeletal muscle adaptation. *Cell Metab* 17: 162–184, 2013.
14. **Garber AJ, Karl IE, Kipnis DM.** Alanine and glutamine synthesis and release from skeletal muscle. *J Biol Chem* 251: 826–835, 1976.
15. **Gibala MJ, MacLean DA, Graham TE, Saltin B.** Anaplerotic processes in human skeletal muscle during brief dynamic exercise. *J Physiol* 502: 703–713, 1997.
16. **Gladden LB.** Lactate metabolism: a new paradigm for the third millenium. *J Physiol* 558: 5–30, 2004.
17. **Golman K, Zandt R, Thaning M.** Real-time metabolic imaging. *Proc Natl Acad Sci USA* 103: 11270–11275, 2006.
18. **Goodyear LJ, Kahn BB.** Exercise, glucose transport and insulin sensitivity. *Annu Rev Med* 49: 235–261, 1998.
19. **Granata AL, Midrio M, Corsi A.** Lactate oxidation by skeletal muscle during sustained contraction in vivo. *Pflügers Arch* 366: 247–250, 1976.
20. **Harris T, Eliyahu G, Frydman L, Degani H.** Kinetics of hyperpolarized $^{13}C_1$-pyruvate transport and metabolism in living human breast cancer cells. *Proc Natl Acad Sci USA* 43: 18131–18136, 2009.
21. **Henriksson J.** Effect of exercise on amino acid concentrations in skeletal muscle and plasma. *J Exp Biol* 160: 149–165, 1991.
22. **Hu S, Balakrishnan A, Bok RA, Anderton B, Larson PEZ, Nelson SJ, Kurhanewicz J, Vigneron DB, Goga A.** ^{13}C-pyruvate imaging reveals alterations in glycolysis that precede c-Myc-induced tumor formation and regression. *Cell Metab* 14: 131–142, 2011.
23. **Jóhannesson H, Macholl S, Ardenkjaer-Larsen JH.** Dynamic Nuclear Polarization of [1-^{13}C]pyruvic acid at 4.6 tesla. *J Magn Reson* 197: 167–175, 2009.
24. **Leto D, Saltiel AR.** Regulation of glucose transport by inuslin: traffic control of GLUT4. *Nat Rev* 13: 383–396, 2012.
25. **Lindblom P, Rafter I, Copley C, Andersson U, Hedberg JJ, Berg A, Samuelsson A, Hellmold H, Cotgreave I, Glinghammar B.** Isoforms of alanine aminotransfereance in human tissues and serum-differential tissue expression using novel antibodies. *Arch Biochem Biophys* 466: 66–77, 2007.
26. **Masad IS, Grant SC.** A retunable surface coil for high field ^{31}P and ^{1}H magnetic resonance evaluations of the living mouse leg. *Physiol Meas* 32: 1061–1081, 2011.
27. **Merritt ME, Harrison C, Sherry AD, Malloy CR, Burgess SC.** Flux through hepatic pyruvate carboxylase and phosphoenolpyruvate carboxykinase detected by hyperpolarized ^{13}C magnetic resonance. *Proc Natl Acad Sci USA* 47: 19084–19089, 2011.
28. **Petersen KF, Shulman GI.** Cellular mechanism of insulin resistance in skeletal muscle. *J R Soc Med* 95: 8–13, 2002.
29. **Py G, Lambert K, Perez-Martin A, Raynaud E, Préfaut C, Mercier J.** Impaired sarcolemmal vesicle lactate uptake and skeletal muscle MCT1 and MCT4 expression in obsese Zucker rats. *Am J Physiol Endocrinol Metab* 281: E1308–E1315, 2001.
30. **Röckl KS, Witczak CA, Goodyear LJ.** Signaling mechanisms in skeletal muscle: acute responses and chronic adaptations to exercise. *IUBMB Life* 60: 145–153, 2008.
31. **Rose AJ, Richter EA.** Skeletal muscle glucose uptake during exercise: how is it regulated? *Physiology* 20: 260–270, 2005.
32. **Ruderman NB.** Muscle amino acid metabolism and gluconeogenesis. *Annu Rev Med* 26: 245–258, 1975.
33. **Schroeder MA, Atherton HJ, Ball DR, Cole MA, Heather LC, Griffin JL, Clarke K, Radda GK, Tyler DJ.** Real-time assessment of Krebs cycle metabolism using hyperpolarized ^{13}C magnetic resonance spectroscopy. *FASEB J* 23: 2529–2538, 2009.
34. **Schroeder MA, Cochlin LE, Heather LC, Clarke K, Radda GK, Tyler DJ.** In vivo assessment of pyruvate dehydrogenase flux in the heart using hyperpolarized carbon-13 magnetic resonance. *Proc Natl Acad Sci USA* 19: 12051–12056, 2008.
35. **Shulman RG, Rothman DL.** ^{13}C NMR of intermediary metabolism: implications for systemic physiology. *Annu Rev Physiol* 63: 15–48, 2001.
36. **Shulman RG, Rothman DL.** The "glycogen shunt" in exercising muscle: a role for glycogen in muscle energetics and fatigue. *Proc Natl Acad Sci USA* 98: 457–561, 2001.